Combining brain-wide activity imaging with electron microscopy reveals a distributed nociceptive network in the brain

Nadine Randel*#, Chen Wang*, Michael S Clayton, Kun Wang, Song Pang, C. Shan Xu, Andrew Champion, Harald F Hess, Albert Cardona[c], Philipp J Keller[c] and Marta Zlatic[c†]

Affiliation:
Nadine Randel: University of Cambridge, University of Cambridge, Department of Zoology, Cambridge CB2 3EJ, United Kingdom
nr479@cam.ac.uk

Chen Wang: Janelia Research Campus, Ashburn, VA 20147, United States
wangc11@janelia.hhmi.org

Michael S Clayton: MRC Laboratory of Molecular Biology, Cambridge CB2 0QH, United Kingdom; mclayton@mrc-lmb.cam.ac.uk

Kun Wang: MRC Laboratory of Molecular Biology, Cambridge CB2 0QH, United Kingdom; kwang@mrc-lmb.cam.ac.uk

Song Pang: Janelia Research Campus, Ashburn, VA 20147; Yale School of Medicine, New Haven, CT 06511; song.pang@yale.edu

C. Shan . Xu: Janelia Research Campus, Ashburn, VA 20147; Department of Cellular and Molecular Physiology, Yale School of Medicine, New Haven, CT 06520; c.shan.xu@yale.edu

Andrew Champion: MRC Laboratory of Molecular Biology, Cambridge CB2 0QH, United Kingdom; achampion@mrc-lmb.cam.ac.uk

Harald F Hess: Janelia Research Campus, Ashburn, VA 20147, United States; hessh@janelia.hhmi.org

Albert Cardona: MRC Laboratory of Molecular Biology, Cambridge CB2 0QH, United Kingdom; University of Cambridge, Department of Physiology, Development and Neuroscience, Cambridge CB2 3EL, United Kingdom; acardona@mrc-lmb.cam.ac.uk

Philipp J Keller: Janelia Research Campus, Ashburn, VA 20147, United States; kellerp@janelia.hhmi.org

Marta Zlatic: MRC Laboratory of Molecular Biology, Cambridge CB2 0QH, United Kingdom; University of Cambridge, Department of Zoology, Cambridge CB2 3EJ, United Kingdom; mzlatic@mrc-lmb.cam.ac.uk

Corresponding author
* Equal contribution
†Lead contact
c Corresponding last author

Abstract

To understand how brains work, it is necessary to connect neural activity to synaptic-resolution circuit architecture. Recent advances in light-sheet microscopy (LSM) enable whole-brain, cellular-resolution imaging of activity of all neuronal cell bodies, however, most neurons from such datasets cannot be identified. In most organisms, neurons are identifiable based on their projections (and not based on their cell body position) which, when densely labelled, cannot be resolved using LSM. Here, we present a novel methodology to overcome this by combining whole-brain activity imaging with subsequent volume electron microscopy imaging of the same brain to visualise neuronal projections and identify neurons with interesting activity. We used this approach to identify brain neurons involved in nociception in *Drosophila* larva. After whole-brain imaging of activity during nociceptive stimulation, we imaged the same brain with an enhanced focused ion-beam electron microscope (eFIB-SEM). We registered the functional and anatomical volumes and reconstructed (in the eFIB-SEM volume) the projections of neurons that responded to nociceptive stimulation to determine their developmental lineage and identity. This revealed a distributed nociceptive network spanning 25 distinct lineages and many distinct brain areas, and included direct brain targets of nociceptive projection neurons that integrate nociceptive information with other sensory modalities, as well as brain output neurons (descending neurons [DN]) that likely contribute to action-selection. Our workflow provides a powerful framework for mapping neuronal activity onto structure across an entire brain, yielding novel insights into the distributed central processing of noxious stimuli.

Introduction

In order to behave adaptively in the environment, animals must process incoming sensory information and select appropriate actions, but we still lack a comprehensive understanding of neural circuits that underlie these fundamental brain functions. One major challenge is that even seemingly simple behaviours, such as responses to innately aversive stimuli, are flexible and subserved by circuits that are not restricted to small, specific brain regions but distributed across many areas of the central nervous system.

Our understanding of neuronal mechanisms has been greatly advanced by access to whole-brain connectomes, which reveal the patterns of connections between all neurons in the brain (White *et al.*, 1986; Ryan, Lu and Meinertzhagen, 2016; Zheng *et al.*, 2018; Verasztó *et al.*, 2020; Witvliet *et al.*, 2021; Takemura *et al.*, 2023; Winding *et al.*, 2023; Azevedo *et al.*, 2024; Dorkenwald *et al.*, 2024). However, while synaptic-resolution connectivity maps are essential for understanding how neural circuits implement fundamental brain functions, by themselves they are not sufficient. To gain a mechanistic understanding of circuit function, in addition to knowing their connectivity patterns, it is also necessary to characterise neuronal activity patterns during a range of behavioural tasks. Indeed, numerous previous studies have shown the importance of linking both synaptic connectivity and neuronal activity on a single cell level to gain a detailed mechanistic understanding of neural circuit mechanisms (Bock *et al.*, 2011; Briggman, Helmstaedter and Denk, 2011; Ohyama *et al.*, 2015; Jovanic *et al.*, 2016; Verasztó *et al.*, 2017; Eschbach *et al.*, 2020, 2021; Toyoshima *et al.*, 2020; Yemini *et al.*, 2021; Svara *et al.*, 2022; Jokura *et al.*, 2023; Lin *et al.*, 2023; Randi *et al.*, 2023; Calderón, Shahidi and Jékely, 2024; Kuan *et al.*, 2024; Boulanger-Weill *et al.*, 2025; Endo *et al.*, 2025).

However, most studies use genetic tools to selectively label and analyse response properties of one identified neuron type at a time. By combining recordings from different neurons, populations, or regions from many different animals during the same task, information about response properties from different neurons can slowly be accumulated. The problem with this approach is that it is very slow, and it would take a very long time to obtain information from all neuron types, during the same tasks. Furthermore, correlations in activity between different neuron types in the same individual cannot be properly assessed.

Recently, advances in light-sheet microscopy (LSM) have opened doors to imaging activity of all neurons in the entire brain of relatively small animals with single cell resolution, including nematodes, insects, and even small vertebrates (Ahrens *et al.*, 2013; Kato *et al.*, 2015; Lemon *et al.*, 2015; Nguyen *et al.*, 2016). Such datasets can comprehensively reveal all neuronal cell bodies with specific response properties. However, in most brains larger than *C. elegans* (where such studies have been extremely fruitful), including those of small insects, like *Drosophila* larvae, cell body position is insufficient to identify neurons (Schrödel *et al.*, 2013; Nguyen *et al.*, 2016). It is, therefore, impossible to combine information about activity of specific neurons from such datasets with previously available information about these neurons–such as their developmental origin (lineage), projection pattern, synaptic connectivity, or molecular properties. In contrast to cell body position, most neurons can be uniquely identified based on the shape and location of their projections. However, while LSM provides sufficient resolution to resolve densely labelled cell bodies from each other (each about 5 µm in diameter), it does not provide sufficient resolution to resolve densely labelled neuronal projections in neuropil areas.

We have therefore developed a methodology that enables us to visualise the projections of all neurons after imaging their activity with LSM, in order to identify neurons based on their projections and combine this information with known information about their connectivity and other properties. Our approach involves imaging the same nervous system with electron microscopy (EM) after whole-brain imaging of neural activity. EM can provide sufficient resolution to resolve densely labelled projections of all neurons in the nervous system, and

identify neurons based on their projection patterns after segmenting large axonal and dendritic branches. Furthermore, recent advances in EM enable imaging entire brains of small animals relatively rapidly. For example, a brain of a *Drosophila* larva (100 µm x 100 µm x 80 µm) can be imaged in one go, in under ten days, with 8 x 8 x 8 nm/voxel resolution with a single enhanced focused ion-beam electron microscope (eFIB-SEM), and other methods allow for even faster imaging of larger brains (Eberle *et al.*, 2015; Xu *et al.*, 2017; Phelps *et al.*, 2021).

We applied this approach to identifying novel elements of nociceptive circuits in the brain of the tractable insect model system, the *Drosophila* larva. The *Drosophila* larva is an excellent model system for brainwide analysis of neural circuit structure and function and for elucidating the circuit mechanisms of fundamental brain functions. Larvae have a rich behavioural repertoire, the complete synaptic-resolution connectome of the *Drosophila* larval brain has recently been published, and a large genetic toolkit is available for selectively targeting and manipulating individual neuron types and elucidating their roles in behaviour (Li *et al.*, 2014; Vogelstein *et al.*, 2014; Ohyama *et al.*, 2015; Almeida-Carvalho *et al.*, 2017; Eichler *et al.*, 2017; Thum and Gerber, 2019; Eschbach and Zlatic, 2020; Eschbach *et al.*, 2020, 2021; Winding *et al.*, 2023; Meissner *et al.*, 2025).

Larval nociceptive circuits have been extensively studied and multiple neurons that respond to noxious stimuli and contribute to innate escape responses have been identified in the ventral nerve cord (Ohyama *et al.*, 2015; Hu *et al.*, 2017; Takagi *et al.*, 2017; Burgos *et al.*, 2018; Dason *et al.*, 2020). Interestingly, these studies, as well as the connectome, have revealed that nociceptive information is relayed to the brain via ascending projection neurons that are also activated by nociceptive stimuli and that facilitate innate escape responses (Ohyama *et al.*, 2015; Winding *et al.*, 2023). However, the number and types of brain neurons that respond to noxious cues, their lineage identity, and whether and how they contribute to innate responses to noxious cues is unknown.

Here, we first imaged calcium transients of all neurons in the larval brain using multi-view LSM while providing targeted stimulation of the primary nociceptive interneurons in the nerve cord. Subsequently, we imaged the same brain with an eFIB-SEM (imaged at 12 x 12 x 12 nm/voxel resolution), registered the LSM and eFIB-SEM volumes of the same brain to each other, and reconstructed the large projections of all neurons that had significant responses to noxious cues, to reveal their developmental origin (lineage identity), and then traced finer branches for a subset of them to uniquely identify them. We then validated our approach by using GAL4-lines to selectively express GCaMP in the identified brain neurons and confirm they respond to noxious stimuli, as revealed by pan-neuronal imaging of activity (Meissner *et al.*, 2025).

Our unbiased comprehensive approach provided novel insights into nociceptive circuits. We found about 4% of brain neurons responded significantly to activation of nociceptive neurons, most of which were previously not known to respond to nociceptive stimuli. The newly identified neurons that responded to nociceptive stimuli spanned a range of neuron categories, including brain neurons that receive input from somatosensory projection neurons, brain output neurons (descending neurons [DN] that project to the suboesophageal zone [SEZ] and the ventral nerve cord [VNC]), as well as neurons presynaptic to the brain output neurons (pre-DN). Surprisingly, we also found that some neurons previously implicated in processing olfactory stimuli (lateral horn neurons, [LHNs]) and some neurons of the higher-order learning circuit implicated in processing conditioned stimuli (a subset of mushroom body Kenyon cells [KCs] and mushroom body output neurons [MBONs]), responded to nociceptive cues.

In summary, this study reveals novel insights into the distributed processing of nociceptive stimuli in the insect brain. The lineages and neurons identified here provide a valuable resource for future studies of the way in which nociceptive cues are integrated with other sensory modalities and used to guide behaviour. Furthermore, the methodology developed in this study will enable overlaying activity patterns during a range of different behavioural tasks

onto the connectome and provides a basis for a comprehensive brainwide understanding of neural circuit function.

Methods

Fly lines

Whole-brain calcium imaging: Flies expressed UAS-RGECO1a pan-neuronally for monitoring neuronal activity, and LexAop-Chronos in the primary nociceptive interneurons, Basins (72F11-LexAp65), for optogenetic activation (Jenett *et al.*, 2012; Klapoetke *et al.*, 2014; Ohyama *et al.*, 2015; Dana *et al.*, 2016).

The final cross LexAop-Chronos (attP18)/ +/Y; 72F11-LexA (JK22)/ UAS-H2B-GFP (attP5); UAS-RGECO1a (VK0005)/ 57C10-GAL4 (attP2) was made by using the following stocks: 13XLexAop2 IVS p10 Chronos mVenus (attP18), 72F11-LexAp65 (JK22C), and 20XUAS-IVS-NES-jRGECO1a-p10 (VK00005) from public collection at HHMI Janelia Research Campus (Ashburn, VA, US); 20XUAS-H2B-GFP-p10 in su(Hw)attP5 gift from Wilhelm Lemon - Philipp Keller lab, HHMI Janelia Research Campus (Ashburn, VA, US); and 57C10-GAL4 (attP2) from Marta Zlatic lab - MRC LMB (Cambridge, UK) (Jenett *et al.*, 2012; Ohyama *et al.*, 2015; Meissner *et al.*, 2025).

Two-photon imaging:
Neuronal activity was recorded from specific cells expressing GCaMP8s during optogenetic activation of Basins that express CsChrimson (Chen *et al.*, 2013; Klapoetke *et al.*, 2014; Zhang *et al.*, 2023).
Crosses were made using the following stocks: 72F11-LexAp65 in JK22C; 20xUAS-IV-GCaMP8s 15.641 in attp2, 13XLexop2-CsChrimson-tdTomato in VK00005 crossed with the GAL4 for DNsez-1 and CSD, and the 14H06-GAL4 line w;14H06-LexAp65 in JK22C;13XLexAop2-IVS-GCaMP8s-p10 50.641 in VK00005, 20XUAS-CsChrimson-mCherry-trafficked in su(Hw)attP1 with 72F11-GAL4 in attp2 (Jenett *et al.*, 2012; Meissner *et al.*, 2025).

Behavioural experiments:
Larval behaviour was recorded with a custom-made rig before and during optogenetic activation of Basins and/or Kenyon cells (Vogelstein *et al.*, 2014). The cross of w;72F11-lexAp65 in JK22C, 72F11-lexAp65 in attp40; 13XLexAop2-IVS-CsChrimson.tdTomato in VK00005/TM6B to 20XUAS-IVS-Syn21-A1ACR1-EYFP-p10 in attP18;;14H06-GAL4 in attP2/TM6B was used as the experimental group while the control group to 14H06-GAL4 in attP2 (Bushey *et al.*, 2025).

Light-sheet microscopy

Sample preparation

Flies were raised on standard fly food. For the experiments, eggs were incubated at 25ºC on standard fly food with 0.5 mmol/l retinal. First instar larvae were dissected in physiological saline solution (Marley and Baines, 2011), and embedded in 1% low-melting temperature agarose (Sigma Aldrich Low melting agarose TYPE VII-A , Sigma (A0701)) in the physiological saline solution, as described in (Lemon *et al.*, 2015).

Data acquisition and processing

The sample was imaged using a multi-view (SiMView) light-sheet microscope at HHMI Janelia Research Campus (Tomer *et al.*, 2012; Lemon *et al.*, 2015). Volumetric imaging was

performed at volume rate of 2.87 Hz and with a voxel size of 0.406 × 0.406 × 1.7 µm. A 561 nm laser was used for fluorescence excitation for the purpose of whole-brain imaging, while a 488 nm laser coupled into one of the microscope's detection arms using a dichroic mirror was concurrently used for optogenetic activation of Basin neurons.

The optogenetic activation protocol alternated between 2 s and 5 s periods of optogenetic stimulation, with a 200 s pause between successive stimulation periods (n = 18). The resulting datasets were processed using a custom analysis pipeline as previously described (Tomer *et al.*, 2012; Lemon *et al.*, 2015).

Electron microscopy sample preparation and imaging

After functional imaging, the sample was immediately prepared for EM volume acquisition (sample ID: 1099). It was fixed in 4% glutaraldehyde in 0.1 M sodium cacodylate buffer (pH 7.4) for 1h at 4ºC, and left in the agarose cylinder during the whole preparation. All washing steps were carried out with 0.1 M sodium cacodylate buffer, until the thiocarbohydrazide step, when water was used.

Post-fixation was performed with 1.25% potassium hexacyanoferrate (II) trihydrate, 1% OsO_4 in 0.1 M sodium cacodylate buffer for 30 min at 4ºC. Next, the sample was incubated for 10 minutes in 1% filtered thiocarbohydrazide in water at room temperature, followed by 1% uranyl acetate in water overnight at 4ºC. Afterwards, the sample was incubated in pre-warmed Walton's lead aspartate for 1 h at 60ºC (Walton, 1979). Finally, the sample was incubated in 0.8% OsO_4 for 30 min on ice. Following that step, the sample was dehydrated in acetone and embedded in Durcupan resin (EMS14040). The Durcupan block was finally mounted on customised soft-copper studs, which are required for the modified eFIB-SEM pipeline (Xu *et al.*, 2017). After trimming and coating with 10 nm gold and 100 nm carbon, the whole sample was imaged at 12 x 12 x 12 nm/voxel.

Landmark-based registration of EM and LSM volume

To translate points between EM and LSM coordinate spaces, we identified 51 shared landmarks in the brain lobes using BigWarp (Bogovic *et al.*, 2016). The landmarks were selected, according to cell morphology and arrangement based on the moving and fixed points from the EM and LSM spaces, respectively. We calculated a thin-plate spline transformation (TPS) using the Thin Plate Spline Python library (https://github.com/raphaelreme/tps) with zero regularization (α = 0.0).

Soma segmentation

Somas in the EM volume were segmented using a convolutional neural network (Stardist) (Schmidt *et al.*, 2018) and trained using a manually annotated dataset of raw images and soma segmentation masks. This process identified 11,596 putative cells across the imaged sample. The centroid of each EM soma was then determined using scikit-image functions (van der Walt *et al.*, 2014), and projected into the light-sheet volume using the previously described TPS transformation. The LSM-projected centroids were then used to generate soma segmentations in the light-sheet volume. To do this, a 3µm^3 sphere mask (corresponding to the average soma size in larval *Drosophila*) was defined and positioned at the central location of every soma. Once applied to every cell, this process generated an instance segmentation of every soma in the LSM volume, based on the initial EM segmentation.

Extraction of neuronal activity

To extract the calcium fluorescence for each soma, the LSM data was first spatially filtered to reduce low-spatial frequencies in each volume, and therefore reduce signal blur between

neighbouring cells. To do this, unsharp masking was applied to each LSM volume in time using the unsharp_mask function in scikit-image (radius=5.0, amount=6.0). For each cell, the mean calcium fluorescence was extracted by calculating the mean intensity across all voxels belonging to the cell for each point in time. This generated a time-series of spatially-filtered fluorescence values for each cell. Further analyses focused only on somas in the brain and supraesophageal zone (SEZ). To do this, a bounding box was drawn around these regions and all somas positioned outside of this box were excluded (i.e. those belonging to cells in the nerve cord). This process resulted in a total of 3,480 remaining neurons.

To study soma calcium responses to Basin stimulation, we calculated stimulus-evoked calcium traces for every cell. For each stimulus delivery (n=18), fluorescence values were taken from ~5 s before and ~5 s after stimulus onset (pre-window=15 frames; post-window=15 frames; imaging frequency=2.87 Hz). For every cell, stimulus-evoked fluorescence values were normalised to the pre-stimulus baseline using the following equation:

$$\frac{\Delta F}{F_0} = \frac{F_{\text{stimulus}} - F_0}{F_0}$$

$F_{stimulus}$ is the mean fluorescence value during stimulus delivery, while F_0 is the mean calcium signal during the ~5 s before stimulus delivery. For every cell and stimulus delivery, the average fluorescence throughout the stimulus-delivery period was calculated (called 'stimulus responses' from here on).

Statistical analysis for whole-brain functional imaging

The reliability of cell responses to Basin stimulations were assessed by performing a one-samples t-test on the distribution of stimulus responses for each cell, assessing whether the sample mean differed significantly from 0. Given the large number of neurons, and therefore statistical tests, p-values were corrected for false discovery rate using the Benjamini–Hochberg (negative) procedure (Benjamini and Hochberg, 1995) (alpha = 0.1; implemented in the Python package, statsmodels.stats.multitest.multipletests (https://www.statsmodels.org/dev/generated/statsmodels.stats.multitest.multipletests.html)). A total of 119 cells had p-values lower than the adjusted significance threshold, and were therefore identified as responding neurons to be brought forward for further analyses.

Neuron identification

Somas showing statistically significant responses to stimulation were located in the EM volume of the sample brain. The axons of selected somas were manually reconstructed using CATMAID (Saalfeld *et al.*, 2009). To identify the cells, neurons of the same lineage were reconstructed until lineage identity could be established. By comparing lineages and neurons across the sample and reference brain, cell lineage and single-cell identity was determined.

Reconstruction of neurons in eFIB-SEM volume

Neurons in the registered 12 x 12 x 12 nm/pixel resolution eFIB-SEM volume were manually reconstructed using CATMAID, as previously described (Saalfeld *et al.*, 2009; Winding *et al.*, 2023).

Synaptic connectivity and circuit analysis of identified neurons

Once neurons were reconstructed in the eFIB-SEM volume and identified based on their morphological similarity to neurons in the previously published reference volume (Winding *et al.*, 2023), the synaptic connectivity and circuitry of identified neurons was analysed in the reference volume, using pymaid with axon-dendritic connections (threshold: 0.01), as previously described (Winding *et al.*, 2023).

Neuron validation

Larval Dissection and Mounting

Central nervous systems (CNSs) of third instar *Drosophila* larvae were dissected in cold saline composed of 103 mM NaCl, 3 mM KCl, 5 mM TES, 26 mM $NaHCO_3$, 1 mM NaH_2PO_4, 8 mM trehalose, 10 mM glucose, 2 mM $CaCl_2$, and 4 mM $MgCl_2$, with an osmolarity of 285 mOsm/L and pH ~7.2. Dissected brains were mounted onto a small piece of cover glass coated with poly-L-lysine (P1524; Sigma) and placed in a 35 mm petri dish lid (Falcon Easy Grip Style; Code: 351008; Scientific Laboratory Supplies), with the brain hemispheres facing upwards.

Two-Photon Imaging and Optogenetic Stimulation

A mode-locked Ti:Sapphire femtosecond pulsed laser (Spectra-Physics), tuned to 920 nm, was used for GCaMP8s imaging. Fluorescence was detected with two photomultiplier tubes (Hamamatsu) following band-pass filtering. Larval brains were imaged at 44 frames per second (fps) in a single focal plane using a two-photon microscope equipped with a fast resonant/galvo scan module (Bergamo, Thorlabs), controlled via ScanImage 2022 (http://www.scanimage.org).

Optogenetic stimulation was delivered via a high-power red LED (4-Wavelength High-Power LED Source; Thorlabs), illuminating the targeted neurons through the main optical path of the Bergamo microscope and a 25× water immersion objective (NA 1.1, WD 2 mm; Nikon). Light stimuli were delivered for 10 s (CSD), 3 s (DNsez-1), and 5 s (Kenyon cells) with an interstimulus interval of 20 s (CSD), 27 s (DNsez-1), and 15 s (Kenyon cells). Each trial consisted of four stimulations, automatically triggered by ScanImage 2022.

Image Analysis

Image time series were processed in Fiji (https://imagej.net/software/fiji/) and further analysed using custom scripts in MATLAB R2022a (The MathWorks, Inc). Regions of interest (ROIs) were manually defined based on the standard deviation projection of the entire time series. A background ROI was also selected outside the target cell region in each dataset to control for LED light bleed-through into the PMT for the green channel. Fluorescence signals in target ROIs were corrected by subtracting this background signal.

Fluorescence changes ($\Delta F/F_o$) were calculated as $\Delta F/F_o = (F_t - F_o)/F_o$, where F_o is the mean fluorescence over a 2-second period preceding the onset of stimulation, and F_t is the mean fluorescence of the ROI at time t. For each brain, mean $\Delta F/F_o$ was computed across the four consecutive stimulations and averaged over three trials.

Statistical Analysis

Differences in mean fluorescent signals (ΔF/F) between 7 s before and during the optogenetic stimulation were analyzed using a paired-sample t-test. A two-tailed α level of 0.05 was applied. All analyses were conducted in MATLAB R2022a.

Behavioural experiments

Drosophila larvae were tested using the laboratory's custom-designed large-scale behavioral rig for optogenetic activation, as previously described (Vogelstein *et al.*, 2014). For each recording, approximately 40 early third instar larvae were transferred onto a 3% agar plate using a fine paintbrush. Larvae were allowed to crawl freely for ~15 s across the plate prior to recording.

Behavioral responses were assessed during simultaneous optogenetic activation of Basin neurons and optogenetic inactivation of Kenyon cells. In the optogenetic protocol, 625 nm red LED illumination (600 μW/cm²) was initiated 30 s after the start of the recording and maintained for 15 s, followed by a 30 s light-off period. This light-on/light-off cycle was repeated twice.

Rolling behavior, defined as an unambiguous escape response, was detected as previously described and the percentage of animals rolling within the first 5 sec time window after stimulation quantified (Jovanic *et al.*, 2016; Croteau-Chonka *et al.*, 2022; Laurent *et al.*, 2024). To minimize potential confounds arising from habituation, only behavioral responses during the first light-on phase were included in the analysis. Statistical comparisons were performed using a chi-square test with Benjamini–Hochberg correction for multiple comparisons (Benjamini and Hochberg, 1995).

Results

Methodology for overlaying brainwide activity and connectivity maps

In order to identify brain neurons with specific functional response properties in an unbiased and comprehensive way, we developed a methodology for overlaying brainwide activity and connectivity maps (Figures 1A-J, 2A-Y and 3A-T).

We expressed a calcium indicator of neural activity (RGECO1a) ubiquitously, in all neurons, and the optogenetic activator of neural activity (Chronos), selectively in a subset of nociceptive interneurons in the nerve cord, called Basins, which receive direct synaptic input from nociceptive sensory neurons and whose optogenetic activation evokes a strong escape response (Tracey *et al.*, 2003; Ohyama *et al.*, 2015). We imaged the activity of every neuron in the extracted nervous system of a first instar larva with a multi-view LSM, before, during and after optogenetic activation of Basins in the fourth abdominal segment (Figure 1A-B). We presented a total of 18 nociceptive stimuli with 200 s between each stimulation.

Immediately after the functional experiment, we processed the sample for volume EM acquisition, by chemically fixing it, followed by staining using an adapted OTO protocol with lead aspartate to enhance contrast (Seligman, Wasserkrug and Hanker, 1966). We then

imaged the entire CNS with eFIB-SEM at 12 x 12 x 12 nm resolution. This resolution is lower than the 8 x 8 x 8 nm resolution used to image adult fly brains, but we reasoned it could be enough to allow tracing of thicker, proximal (closer to the cell body) neuronal projections (even if not thinner, more distal branches and synapses) (Scheffer *et al.*, 2020). After acquiring the eFIB-SEM volume, we registered the datasets of the two imaging modalities, using 51 landmarks detectable in both volumes (Figure 1D-E, 2A). Based on this registration, the segmented nuclei in the EM volume were projected into the LSM volume to extract their changes in fluorescence at single cell resolution (Figure 2B). Consequently, we were able to locate nuclei in the EM volume whose activity correlated with the optogenetic manipulation of Basin neurons (Figure 2C).

From the ~3000 brain neurons, 119 neurons (~4%) responded consistently and significantly to the activation of Basin neurons (Figure 2C). Interestingly, the cell bodies of many of these neurons were located in the same brain region, as the cell bodies of brain neurons that receive shortest possible, two-hop input from Basins (via direct input from ascending projection neurons directly postsynaptic to Basins) in our recently-published reference brain connectome (Figure 3B) (Winding *et al.*, 2023).

To identify the developmental origin (lineage) of these neurons we manually reconstructed their thick, proximal projections up to their entry point into the neuropil and a little beyond (Figure 2D). Based on their entry point into the neuropil, we identified 25 cell lineages that each contained between 1-30 neurons that responded to nociceptive stimulation (Figure 2E-Y).

Next, we randomly selected 50 of the 119 neurons that responded to Basin activation (Figure 3A) to determine what fraction of them could be uniquely identified based on the intermediate, more distal branches that were traceable in this 12 x 12 12 nm resolution FIB-EM dataset. For this purpose, we traced their thinner branches as far as possible, and then compared the overall shapes of their projections to the shape of the reference neurons from our recently published, complete reconstruction of all neurons in a larval brain [and their synaptic connections] (Winding *et al.*, 2023). We were able to trace intermediate-sized branches for 26/50 neurons (Figure 3A-T), whereas the intermediate-sized branches were not traceable for the remaining 24 neurons, due to the chosen 12 x 12 x 12 nm resolution of eFIB-SEM imaging. We were able to uniquely identify 18/26 individual neurons based on their intermediate-sized branches and 8/26 neurons could be narrowed down to 2 - 4 candidate neurons within the same lineage due to the high morphological similarity of their intermediate-sized branches (Figure 1F, 3C-T). Having identified neurons responsive to nociceptive interneuron activation, we could analyse in detail their connectivity patterns and their direct and indirect upstream and downstream partners (Figure 4A-O).

Finally, to validate our methodology (Figure 5A-P), we searched for available GAL4 lines that selectively target gene expression to these neurons (Meissner *et al.*, 2025). We were able to identify lines for 3 out of the 26 neurons (Figure 5F, 5K and 5O). We used these GAL4 lines to selectively express GCaMP8s in each of these neurons, and imaged their responses to Basin activation using two-photon microscopy (Figure 1G-H and 5G, 5L and 5P) (Chen *et al.*, 2013; Zhang *et al.*, 2023). We confirmed that they all had similar responses when imaged individually, to the responses obtained using whole-brain imaging, thereby validating our ability

to correctly identify neurons after whole-brain imaging of neural activity and confirming the reproducibility of their responses to noxious stimuli across individuals.

Identifying brain neuronal lineages activated by noxious stimuli

The *Drosophila* larval brain contains approximately 100 stereotyped neuronal lineages. Neurons from each lineage derive from a single neuroblast and follow a characteristic trajectory to the neuropil and enter the neuropil at a stereotypic location and project into similar neuropil areas (Spindler and Hartenstein, 2010). The lineage identity of each neuron can therefore be uniquely identified based on the trajectory its axon takes to the neuropil and the neuropil entry point.

To identify the lineage of each of the 119 neurons that significantly responded to Basin activation, we therefore manually traced their axons that lead from the cell body to the neuropil entry point and beyond (Figure 2D-Y). We were able to trace in this way 101/119 neurons (85%), and the remainder could not be traced due to image artifacts affecting some portions of the EM volume. Based on their neuropil entry point, we identified 25 neuronal lineages that each contained between 1 - 30 neurons that responded to nociceptive stimulation (Figure 2E-Y; Table 1).

We wondered whether neurons from lineages that received the most direct Basin input were more likely to respond to Basin activation, than others. Therefore, we analysed the published connectome of the *Drosophila* larval brain (Winding *et al.*, 2023) and found that 82 lineages contain neurons that receive Basin input within ≤5 hops. 25 of these 82 lineages contained neurons that significantly responded to Basin activation in our whole-brain imaging experiment. None of the neurons from lineages that contained neurons that were not connected to Basins with 5 or less hops responded to Basin activation (Table 2)., Only 15 lineages contained neurons that received two-hop input from Basins (via direct input from ascending projection neurons from the nerve cord that in turn receive direct Basin input), but 10 out of these contained neurons that significantly responded to Basin activation (Figure 2E–Y; Table 1). Thus, 40% of the 25 lineages whose neurons responded to Basins received two-hop input from Basins. Overall, our data reveal that neurons from lineages that contain the most direct, two-hop, input from Basins are more likely to respond to Basin activation, than neurons from lineages that receive more indirect input via longer paths: 10/15 (67%) vs. 15/67 (22%).

Next we analysed the activity of the neurons within the same lineage. We discovered that all neurons within a single lineage responded similarly to the stimulus. The activity traces often overlapped, and all neurons were either depolarised or hyperpolarised upon Basin activation. The only exception was the cell lineage BLAv1/2, where 2 out of 30 depolarised cells responded via hyperpolarisation (Figure 2G). The results indicate that the neurons within a lineage mainly respond in a similar fashion, either being depolarised, or hyperpolarised.

The mean and median number of neurons that responded to Basin activation per lineage, was small (5 and 2, respectively). Interestingly, a few lineages contained a large number of neurons that responded to Basins (Figure S1; Table 4): BLAv1/2 (30; 27% of all neurons in that lineage); BLVa3/4 (9 neurons; 9% of neurons in that lineage); BLVp1/p2 (12 neurons; 19% of

neurons in that lineage) and BLD2-4 (17 neurons; 24% of all neurons in that lineage). These four lineages, therefore, contributed 57% of all Basin-responsive neurons in the brain (68/119, 57%). Significant fraction of neurons from these lineages also received two-hop input from Basins via direct input from ascending projection neurons from the nerve cord: 26%, 20%, 23% and 11% of neurons from BLAv1/2, BLVa3/4, BLVp1/p2 and BLD 2-4 (Table 5), respectively, and others receive three-hop input. Our findings therefore identify four lineages as major contributors of neurons that process nociceptive information in the brain.

Identifying individual brain neurons activated by noxious stimuli

Next, we randomly selected 50 neurons that significantly responded to Basin activation to determine what fraction of them we can identify as corresponding to one of the neurons from the reference brain. We traced their fine projections and compared their morphology to the reference neurons from our recently published reconstructions of all larval brain neurons (Winding *et al.*, 2023). In our 12 x 12 x 12 nm/voxel resolution eFIB-SEM dataset, of the selected neurons, we were able to trace 18 cells sufficiently to identify them (DNsez-1, CSD, LHN-32, DNsez-3 left and right, somPN 9, MBON-q1, Noose 1, Tel-like 1, DNvnc-20 left and right, pre-DNvnc-20, DNvnc-13, and five Kenyon cells [KCs]); 8 neurons could be narrowed down to 2-4 candidates with very similar projections belonging to the same neuron types within the same lineage (DNvnc-14-15, somPN 7-8, DNvnc-16-19; two Lasso-top neurons that could each be one of Lasso-top 1-3, but since Lasso-top 1 only receives 7-hop input from Basins, whereas Lasso-top 2 and 3 both receive 5-hop input, it is likely that the identified Basin-responsive neurons are Lasso-top 2-3; and 3 neurons that each could be somPN 6, pre-DNvnc-18, or pre-DNvnc-19 [Figure 3E,F,H,L,N, and Table 2]). The remaining cells could not be traced sufficiently to allow identification. 20/26 identified neurons were depolarised and 6/26 hyperpolarised in response to Basin activation (Figure 3A,C-T, S2; Table 2).

All identified cells receive input from Basins via two to five hops (Table 2), some forming strong hubs (having ≥20 in- or out-degree) within the network, such as DNsez-3, DNsez-1, LHN-32, somPN 8, pre-DNvnc-20 and CSD (Table 2). These neurons integrate information from multiple other neurons of the nociceptive circuit. We also discovered recurrent feedback connections onto Basins from two of the hub neurons (LHN-32 and DNsez-1).

We analysed in more detail the 26 identified neurons (Table 2). Three identified brain neurons receive the shortest possible, two-hop, input from Basins, via direct synaptic input from ascending projection neurons (A00c) that receive direct Basin input: somPN 7-8, somPN 9 , and somPN 6 (Figure 4A). SomPN 9 integrates nociceptive information from the two sides of the body (Figure 4D). SomPN 7-8 also receives direct input from other somatosensory ascending projection neurons (Figure 4B and 4E). These three neurons also integrate nociceptive input with other sensory modalities (gustatory and olfactory via input from lateral horn neurons [LHNs], Figure 4F-G).

Furthermore, somPN 6, somPN 7-8 and somPN 9 directly innervate brain output neurons (DNs), thus participating in short nerve cord-brain loops (Figure 4C; Table 3). Thus, somPN 7-8 and somPN 9 directly innervate the DN-SEZ neuron DNsez-3. SomPN7-8 also directly innervates the identified DNvnc-20.

Overall, one third of the identified neurons that were responsive to Basins were DNs (19% DN-VNC and 12% DN-SEZ), transmitting the signal from the brain to the VNC, or to SEZ (Figure 4H,J, K). This includes five DN-VNC neurons (DNvnc-13, DNvnc-14 or DNvnc-15, DNvnc-16-19, DNvnc-20 left and right), and three DN-SEZ (DNsez-1, DNsez-3 left and right) (Table2). Furthermore, four neurons were pre-descending neurons (pre-DN-VNCs), directly upstream of DNs (CSD, pre-DNvnc-18, pre-DNvnc-19, pre-DNvnc-20).

Three of the identified DNs (DN-vnc-16-19, DN-vnc-20, DN-sez-1) synapse directly or via 2-hops onto Gorogoro, a previously identified command neuron for the rolling escape response, that also receives Basin input via a shorter nerve cord pathways (Figure 4L). The shortest brain pathway from the nociceptive interneuron Basins to Gorogoro is only 4-hops (Figure 4M). Interestingly, we found direct signal integration between Basins and DN-vnc-16-19, onto A05q that innervates Gorogoro (Figure 4N.)

We also found that some neurons previously implicated in processing olfactory stimuli are activated by Basins (a lateral horn neuron, LHN-32), suggesting these neurons are multisensory. Surprisingly, five of the intrinsic neurons (Kenyon Cells [KCs]) of the learning circuit (the mushroom body [MB]), also responded to Basin activation, as did an MB output neuron (MBON-q1) (Thum and Gerber, 2019; Eschbach and Zlatic, 2020)(Kent, Hoskins and Hildebrand, 1987; Eichler *et al.*, 2017). KCs are probably one of the most studied neurons in the *Drosophila* nervous system, but despite this, they were never previously reported to respond to noxious cues, as they are usually thought of as representing conditioned stimuli (CS), such as odours, temperature or light), but not unconditioned stimuli (US) that serve as punishments (such as noxious cues) or rewards during associative learning tasks. We identified a 5-hop synaptic pathway between Basins and KC (Figure 4O).

Finally, four neurons identified in this study as responsive to nociceptive neuron activation, did not belong to any previously known neuron categories (Lasso-top 1-3 neurons, Tel-like 1, Noose 1).

Together, these findings expand our knowledge of nociceptive processing in the insect brain and identify numerous neurons for future follow-up studies.

Validating identified brain neurons

Finally, we wanted to validate our methodology and our findings by confirming that the specific neurons we identified as responding to Basin activation using whole-brain imaging of neural activity, are reproducibly activated by Basins. To do this, we wanted to selectively express a calcium indicator of neural activity in one identified neuron at a time and image their responses to Basin activation in multiple animals. We, therefore, looked for available GAL4 lines that drive expression, selectively, in the neurons that we identified as responding to Basin activation. We were able to find GAL4 lines for 3/26 of the identified neurons: DNsez-1 and CSD, as well as a line that drives expression in all KCs (Kent, Hoskins and Hildebrand, 1987; Coates *et al.*, 2017).

We used these GAL4 lines to express GCaMP8s , selectively in the neurons of interest, and the Basin-LexA to express the optogenetic activator of neural activity, Chrimson, selectively in Basin neurons (Klapoetke *et al.*, 2014; Ohyama *et al.*, 2015; Zhang *et al.*, 2023). We optogenetically activated Basins and imaged the responses of KCs, DNsez-1, and CSD using two-photon microscopy. The results reproduced our findings from the whole brain imaging

experiment, where Kenyon cells and DNsez-1 were depolarised in response to Basin activation, and CSD was briefly depolarised, and then strongly hyperpolarised throughout Basin activation (Figure 3C,D,O, 5A-B, D-P).

Overall, these findings validate our methodology and show we could reproduce findings from whole-brain, pan-neuronal imaging experiments by imaging activity of a single neuron type at a time, with cell-type-specific expression of GCaMP. Whole-brain imaging enabled us to identify many more neurons involved in processing nociceptive stimuli, for which selective driver lines currently do not exist. In the future, whole-brain imaging of neural activity will enable systematic characterisation of response properties of all neurons in the brain, to a range of stimuli and across a range of behavioural tasks.

Kenyon cells contribute to innate behaviour

Perhaps one of the most unexpected findings in our study is that the intrinsic neurons of the MB, the KCs, known to be required for associative learning and memory and thought to represent CS, also respond to nociceptive interneurons whose stimulation serves as an unconditioned aversive reinforcement signal during associative learning tasks (Heisenberg *et al.*, 1985; Eschbach *et al.*, 2021).

We, therefore, wondered whether KCs contribute to innate behaviour, in particular the innate escape response to noxious stimuli. To test this, we optogenetically silenced KCs [using the red-shifted inactivator of neural activity, Ruby (Bushey *et al.*, 2025)], during optogenetic activation of Basin neurons [using the red-shifted activator of neural activity, Chrimson (Klapoetke *et al.*, 2014)] and analyse larval rolling escape response, which is normally induced by Basin activation (Ohyama *et al.*, 2015). We found a mild, but significant reduction in rolling when KCs were silenced, compared to controls, supporting a role for the MB in facilitating the innate escape response (Figure 5C).

This finding highlights further the value of an unbiased whole-brain imaging approach when identifying neuron types involved in specific functions.

Discussion

In this study we developed a novel methodology for identifying neuron types and individual neurons following cellular-resolution, whole-brain imaging of neural activity with LSM. While cell body position alone is not sufficient to identify neurons, most neuron types (and even individual neurons) can be identified based on the locations and shapes of their projections. Our methodology, therefore, involves imaging the same brain with higher-resolution volume EM, to visualise neuronal projections, followed by reconstruction of the branches of those neurons that have interesting activity properties. This approach enables combining information about neuronal activity with previously available information about each neuron, such as their synaptic connectivity, molecular properties, or roles in behaviour.

We applied our approach to gaining a better understanding of the processing of nociceptive stimuli in the brain of *Drosophila* larvae. After pan-neuronal calcium imaging in response to optogenetic activation of nociceptive interneurons (Basins), we imaged the same CNS with eFIB-SEM at 12 x 12 x 12 nm/voxel resolution, sufficient to visualise medium-sized neuronal

branches, and registered the two datasets of the same brain to each other, using landmark-based registration. From the LSM dataset we found that 119 neurons significantly responded to Basin activation. We randomly selected 50 of these neurons for follow up and manually traced their medium-sized branches in the eFIB-SEM volume. Because existing models for automated segmentation of neuronal arbours in *Drosophila* were trained on eFIB-SEM datasets that were imaged with 8 x 8 x 8 nm/voxel resolution (Scheffer *et al.*, 2020), for this proof-of-principle study we manually traced neuron arbours and were, therefore, not able to follow-up all 119 neurons. 26/50 could be traced sufficiently to identify them, either uniquely, or to a neuron type with very similar projections within the same lineage. Finally, we validated our neuron identification using GAL4 lines to selectively drive GCaMP in some of the identified neurons and confirmed they reproducibly respond to optogenetic activation of nociceptive interneurons in multiple individuals.

We also considered how resolution and imaging speed influence the applicability of this approach. Prior studies show that imaging *Drosophila* brains with eFIB-SEM using 8 x 8 x 8 nm/voxel resolution is sufficient to reconstruct neuronal fine branches and synapses (Scheffer *et al.*, 2020; Takemura *et al.*, 2023). Here we chose a lower, 12 x 12 x 12 nm/voxel resolution, to assess the extent to which medium-sized branches will be traceable and the extent to which this would be sufficient for identifying neurons. While, for *Drosophila* larval brains, imaging with 8 x 8 x 8 nm/voxel resolution would be very fast (ten days per brain), imaging with 12 x 12 x 12 nm/voxel resolution is 30% faster, and would enable acquisition of large sample sizes, or faster imaging of larger brains. Overall, our study demonstrated that, after cellular-resolution imaging with LSM, imaging the same brain with 12 x 12 x 12 nm/pixel eFIB-SEM, enables identification of ca. 50% of neurons. In the future, for smaller brains, such as that of *Drosophila* larva, imaging with synaptic-resolution (8 x 8 x 8 nm/voxel) would be fast enough and would provide significant advantages: first, it would enable tracing of fine branches and synapses; second, it would enable automated segmentation of neuronal branches using existing models and therefore identification of most neurons in the brain (Scheffer *et al.*, 2020). As EM imaging and reconstruction gets faster and faster, it may be possible to apply this approach to larger and larger brains (Eberle *et al.*, 2015; Xu *et al.*, 2017; Barsotti, Correia and Cardona, 2021; Phelps *et al.*, 2021). Furthermore, expansion microscopy may also be used instead of EM to visualise neuronal projections following whole-brain imaging of neural activity (Chen, Tillberg and Boyden, 2015; Hörl *et al.*, 2019; Gallagher and Zhao, 2021; Lillvis *et al.*, 2022).

Nociceptive circuits in the *Drosophila* larval nerve cord have been extensively studied, but much less was known about nociceptive signalling in the brain. Here we discovered multiple novel neuron types responsive to nociceptive stimuli. 20/26 (77%) of identified neurons were depolarized and 6/26 (23%) hyperpolarized in response to nociceptive neuron activation. We discovered hub-neurons for nociceptive processing, as well as feedback neurons that signal back to the first-order nociceptive interneurons (Basins), likely modulating their response to noxious stimuli. Identified neurons also included direct targets of nociceptive ascending projection neurons in the brain, some of which integrate nociceptive information from two sides of the body, while others integrate nociceptive information with other sensory modalities, as well as brain descending neurons that project to the premotor regions of the nerve cord and could play a role in facilitating responses to nociceptive stimuli.
Surprisingly, we also discovered nociceptive responses in neuron types and brain areas previously associated with olfactory processing and learnt responses to conditioned stimuli. For example, a subset of KC, the intrinsic neurons of the learning circuit (the MB), responded

to nociceptive interneuron activation. KCs are essential for associative learning, and have been demonstrated to encode conditioned stimuli, such as odours, light, or temperature that can be associated with unconditioned stimuli, such as noxious stimuli (Heisenberg, 2003; Campbell *et al.*, 2013; Dylla *et al.*, 2017; Ganguly *et al.*, 2024; Polizos *et al.*, 2024). Our study shows that a subset of KCs responds to nociceptive stimulation. Indeed, analysing the connectome reveals axo-dendritic paths from Basin neurons to a subset of KCs. Furthermore we found that optogenetic silencing of KCs reduces the likelihood of innate rolling escape response to nociceptive interneuron activation. This suggests that KCs mediate not only learnt behaviour, but also facilitate innate escape response. In the future, it will be interesting to test whether the KCs activated by noxious stimuli also play a role in learning to respond more or less strongly to noxious stimuli depending on experience.

Overall, these findings demonstrate how unbiased, whole-brain imaging approaches can reveal unexpected response properties, even for some of the most studied cell types in the brain. Furthermore, for many of the identified neurons, GAL4 lines are not available, underscoring the importance of whole-brain imaging to study the response properties of a large fraction of neurons for which genetic driver lines are not available.

In summary, our study identified multiple neuron types in the insect brain involved in processing nociceptive stimuli. The methodology we have developed will enable overlaying brainwide activity maps during various behavioral tasks onto connectivity maps, an essential step towards understanding neural circuit function.

Acknowledgements

The authors thank MRC Laboratory of Molecular Biology, HHMI Janelia Research Campus and Department of Zoology, University of Cambridge for funding and support. We thank Bill Lemon (HHMI Janelia Research Campus), Fly core (especially Monti Mercer) at JRC, and Nan Hu and Oxana Elliott at the Department of Zoology, University of Cambridge for fly crosses. We thank the Janelia Visitor Project for outstanding support over the years. We thank MRC Laboratory of Molecular Biology Core funding (MZ, AC, MJW and KW), HHMI Janelia Research Campus (MZ, AC, PJK, NR, CW, HFH, SCX, SP), European Union Horizon 2020, Marie Skłodowska-Curie Grant No 838225 (NR), Wellcome Trust grant 205038/Z/16/Z (AC), Wellcome Trust grant 205050/Z/16/Z (MZ), ERC grant ERC-2018-COG: 819650 (MZ, NR) for funding.

Figures

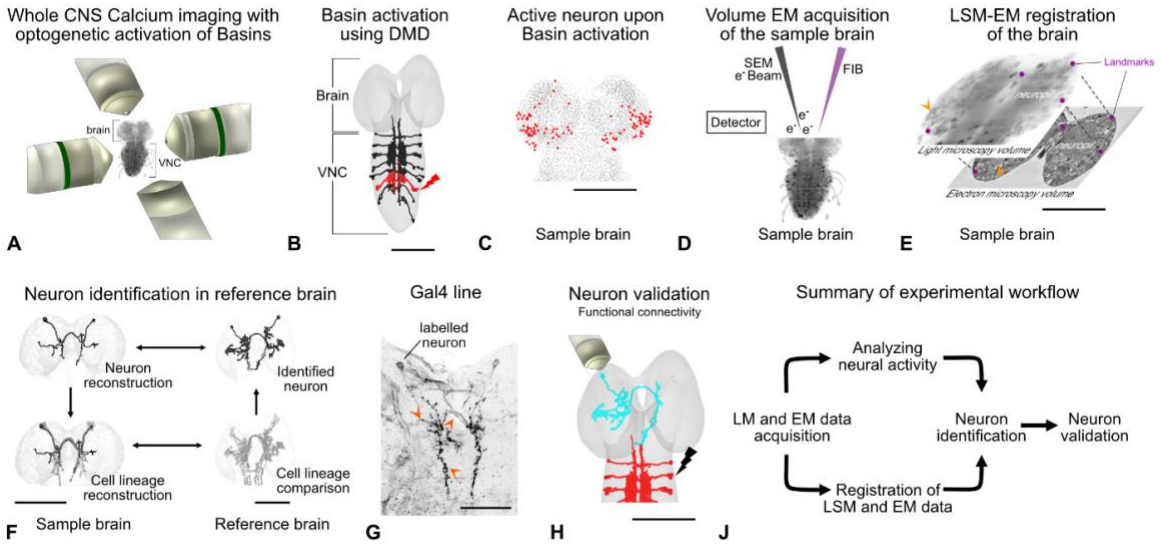

Figure 1: Linking single-neuron activity with synaptic connectivity. A: Whole central nervous system functional imaging with selective optogenetic activation, using multi-view light-sheet microscopy (SiMView). **B:** Optogenetic activation of Basins in the fourth abdominal segment using a digital micromirror device (DMD) coupled into the SiMView microscope. **C:** Location of brain neurons (red) that respond to Basin stimulation. **D:** Volume electron microscopy acquisition of the sample with known neuronal activity from panel A. **E:** Landmark-based registration of light and electron microscopy volumes of the same sample. **F:** Workflow of neuron identification in the sample brain, using the whole-brain reference connectome (Winding *et al.*, 2023). **G:** Genetic driver line of the identified neuron. Arrowheads: Neurite of labelled neurons. **H:** Validation of identified neurons using 2-photon imaging of single neurons with optogenetic activation of Basins. **J:** Workflow to integrate and validate single-cell neuronal activity with synaptic connectivity. Scale bar: 50 µm.

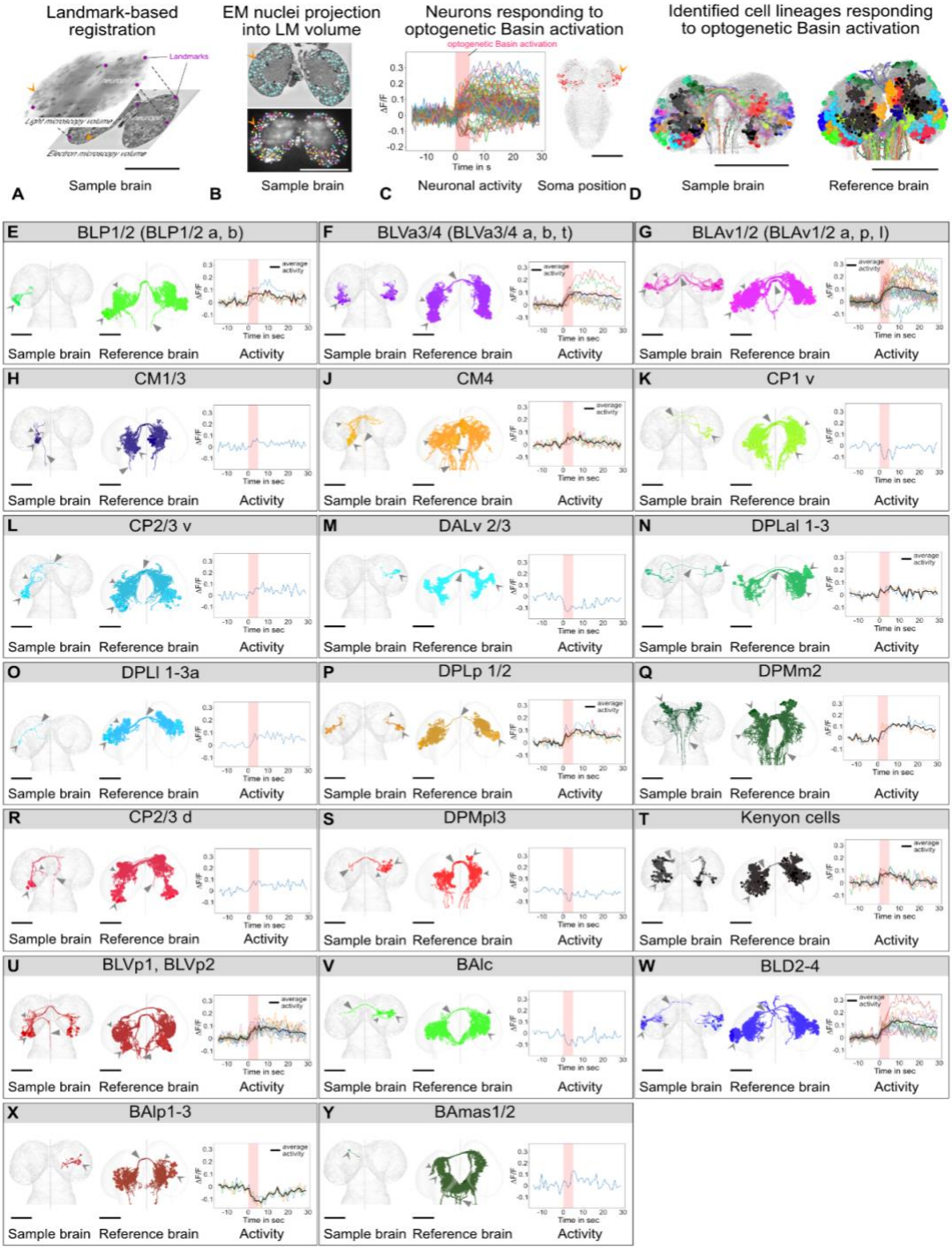

Figure 2: Cell-lineages responding to Basin activation. A: Landmark-based registration of light and electron microscopy volumes of the same sample. **B:** Automatic nuclei segmentation in the electron microscopy volume, and nuclei projection into the registered light microscopy volume. **C:** Activity traces and brain neuron locations that respond to Basin activation (red shading). **D:** Cell lineages responding to Basin stimulation in the sample brain and reference brain. Non-responding lineages are shown in grey. **E-Y:** Individual cell-lineages shown in both the sample and reference brain, with corresponding neuronal activity. Average traces shown in black. Red shading indicates time of optogenetic Basin activation. **G:** Hyperpolarised neurons are shown in a lighter shade. Scale bar: 25 µm. Dashed line indicates the midline, barbed arrowhead shows cell body, triangle indicates axon, and curved arrowhead shows dendrite.

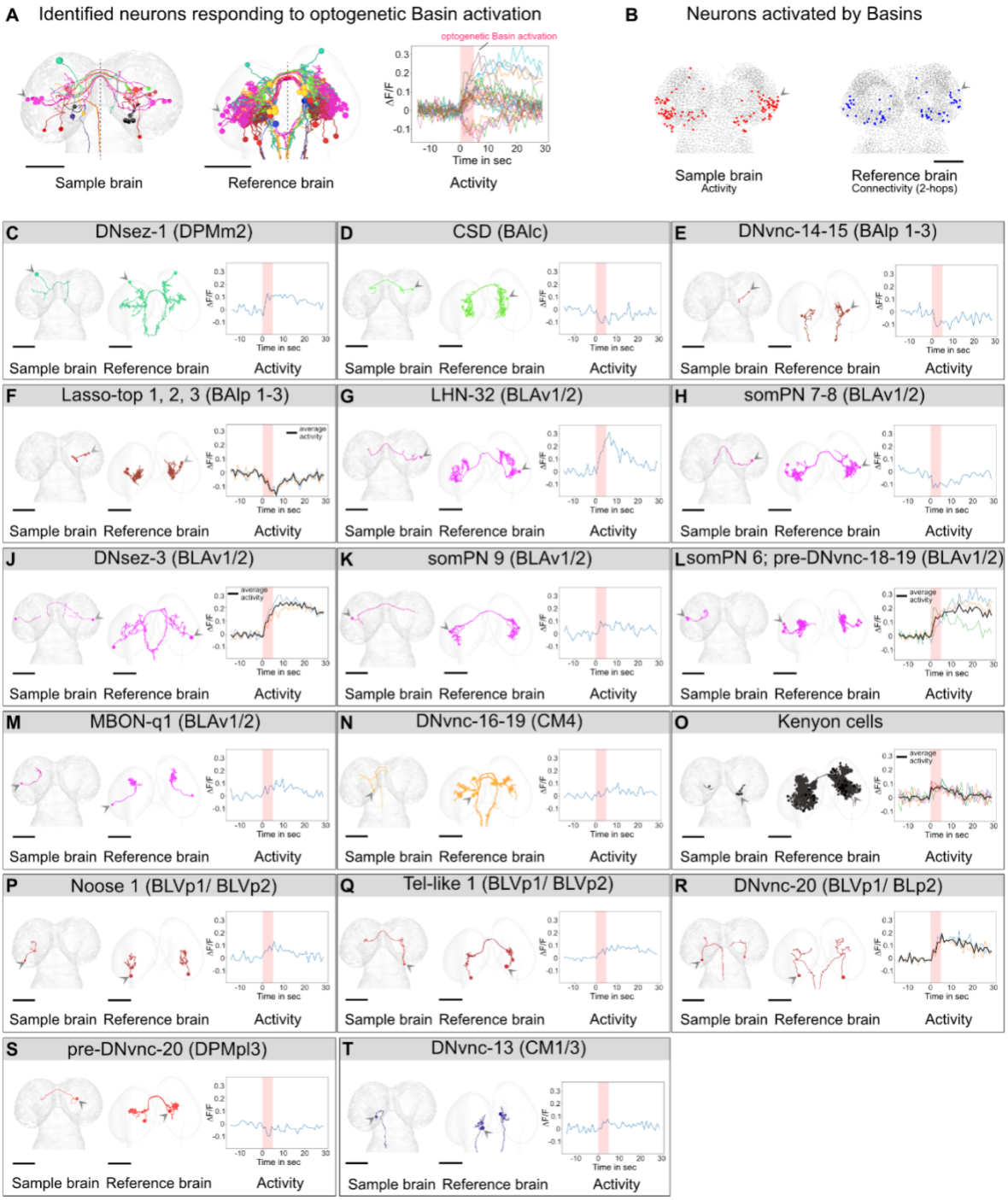

Figure 3: Identified neurons responding to Basin activation. A: Summary of identified neurons in the sample brain and reference brain, with corresponding neuronal activity. Dashed line indicates the midline. **B:** Many neurons responding to Basin activation in the sample brain (left) have similar cell body locations to brain neurons that receive shortest possible, 2-hop input from Basins in the reference connectome. **C-T:** Individual identified neurons shown in both the sample and reference brains, with corresponding neuronal activity. **E,F,H,L,N:** Candidate neurons. Individual identification was not possible due to high neuronal similarity or incomplete reconstruction. Average activity traces shown in black. Barbed arrowhead shows cell body, triangle indicates axon, and curved arrowhead shows dendrite. Scale bar: 25 µm.

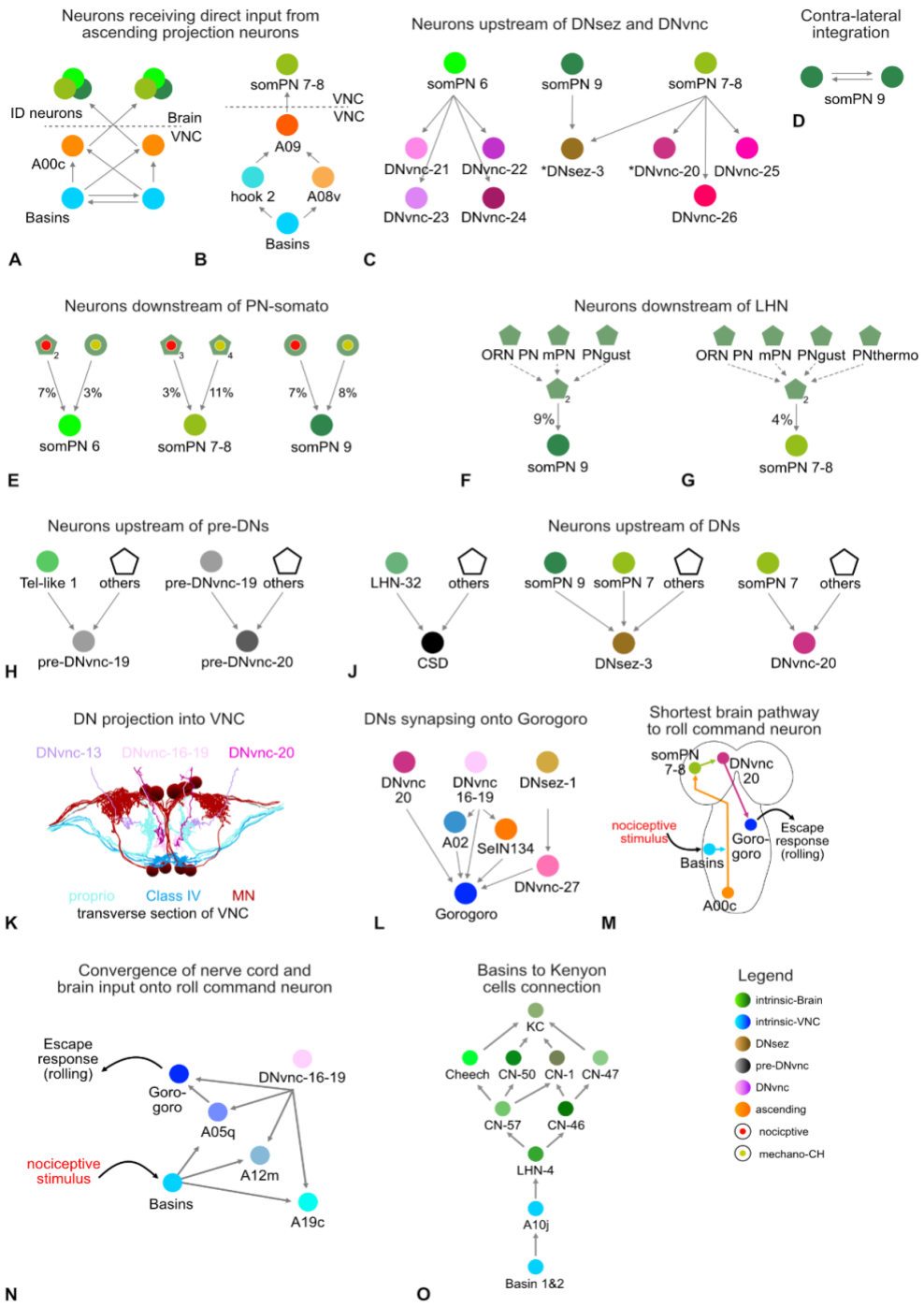

Figure 4: Circuit analysis. A: Shortest neuronal pathway from the VNC to the brain neurons somPN 6, somPN 7-8, and somPN 9 via the ascending neurons A00c. **B:** Path from the VNC to the brain via other ascending neurons. **C:** Brain neurons synapsing on DNs. *Identified neurons. **D:** Bilateral signal integration in the brain. **E:** 1-hop multimodal integration from PNsomato, and **F, G:** lateral horn neurons. Lateral horn neurons receive input from olfactory (ORN), gustatory (PNgust), and multiglomerular (mPN) projection neurons. The polygons indicate a group of neurons and the relative synaptic input. **H:** Brain neurons synapsing onto pre-DNvnc, and **J:** DNvnc neurons. **K:** DNvnc axon location in the VNC. **L:** DNvnc synapsing onto Gorogoro, the command neuron for rolling behaviour. **M:** Shortest nociceptive brain pathway from Basins to Gorogoro. **N:** Integration from Basins and DNvnc neurons. **O:** Neuronal pathway from Basins to Kenyon cells. Synaptic threshold: ≥ 3 synapses.

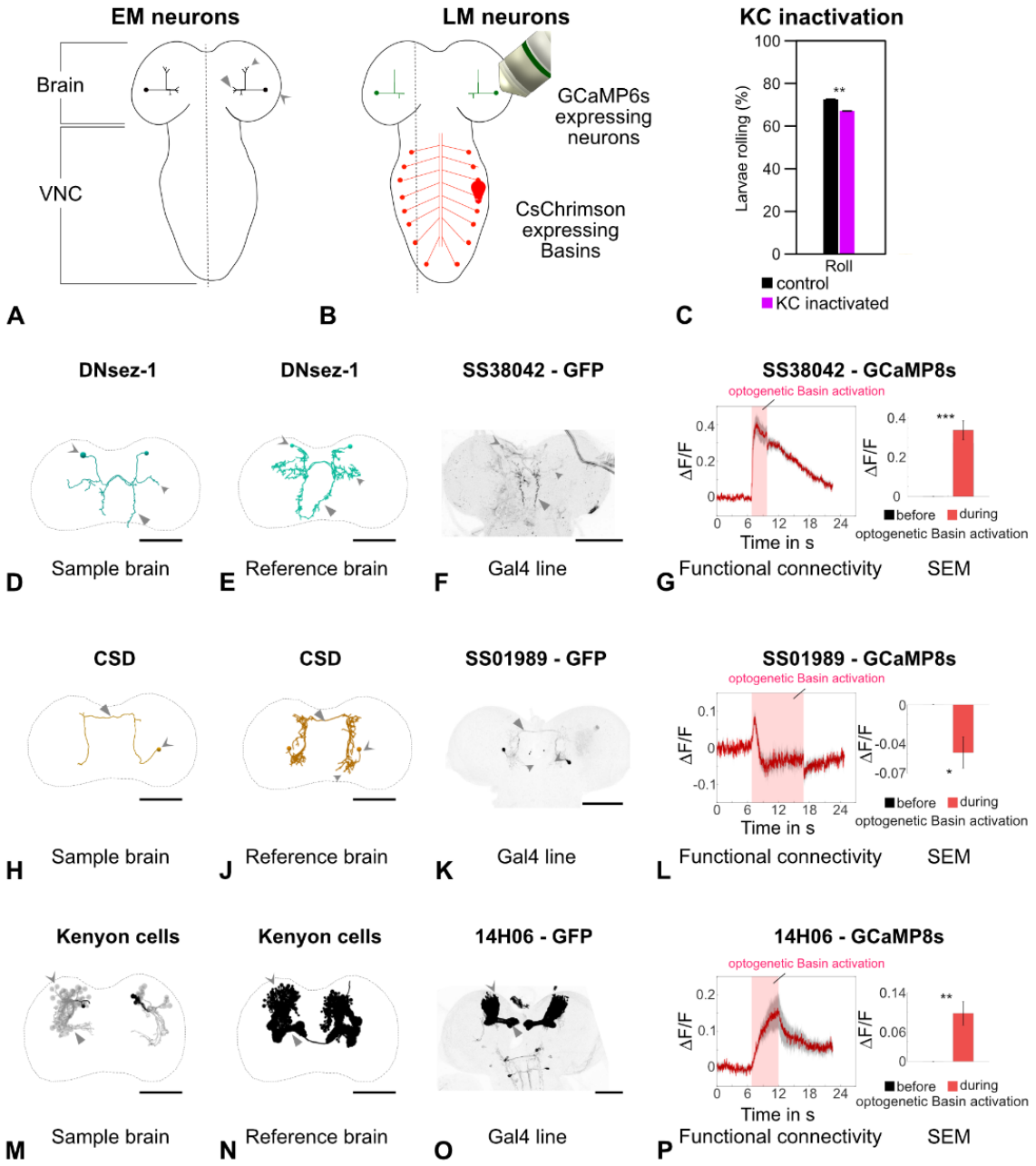

Figure 5: Neuron validation. A: Schematic of identified brain neurons. **B:** Corresponding driver line expressing GCaMP8s. **C:** Nociceptive stimuli evoke less rolling (escape) behaviour during Kenyon cell inactivation [w;72F11-lexAp65; LexAop2-IVS-CsChrimson/ UAS-A1ACR1-EYFP-p10/ 14H06-GAL4] (magenta) compared to control [w;72F11-lexAp65; LexAop2-IVS-CsChrimson/ 14H06-GAL4] (black) larvae. n=450 larvae for the experimental group and n=454 larvae for the control group with both in runs of experiments; p=0.004. Chi-squared test. **D, H, M:** Reconstructed neurons in the sample brain. In **M**, the identified Kenyon cells are in black, and additional Kenyon cells are shown in grey. **E, J, N:** Corresponding neurons in the reference connectome. **F, K, O:** Matching driver lines expressing GFP. **G, L, P:** Neuronal responses to Basin activation recorded via 2-photon microscopy, and bar plot of mean and standard error of the mean (SEM) comparing neuronal activity before stimulus and during the complete stimulus window **(G, P)** or stimulus start +1s **(L)**. Paired-sample t-test. **G:** n=8; p=0.0002. **L:** n=8; p=0.02. **P:** n=11; p=0.002. Scale bar: **D, E, H, J, M, N**: 25 µm; **F, K, O**: 100 µm. Dashed line indicates the midline, barbed arrowhead shows cell body, triangle indicates axon, and curved arrowhead shows dendrite.

References

Ahrens, M.B. *et al.* (2013) ‘Whole-brain functional imaging at cellular resolution using light-sheet microscopy’, *Nature methods*, 10(5), pp. 413–420. Available at: https://doi.org/10.1038/nmeth.2434.

Almeida-Carvalho, M.J. *et al.* (2017) ‘The Ol1mpiad: concordance of behavioural faculties of stage 1 and stage 3 Drosophila larvae’, *The journal of experimental biology*, 220(Pt 13), pp. 2452–2475. Available at: https://doi.org/10.1242/jeb.156646.

Azevedo, A. *et al.* (2024) ‘Connectomic reconstruction of a female Drosophila ventral nerve cord’, *Nature*, 631(8020), pp. 360–368. Available at: https://doi.org/10.1038/s41586-024-07389-x.

Barsotti, E., Correia, A. and Cardona, A. (2021) ‘Neural architectures in the light of comparative connectomics’, *Current opinion in neurobiology*, 71, pp. 139–149. Available at: https://doi.org/10.1016/j.conb.2021.10.006.

Benjamini, Y. and Hochberg, Y. (1995) ‘Controlling the false discovery rate: A practical and powerful approach to multiple testing’, *Journal of the Royal Statistical Society. Series B, Statistical methodology*, 57(1), pp. 289–300. Available at: https://doi.org/10.1111/j.2517-6161.1995.tb02031.x.

Bock, D.D. *et al.* (2011) ‘Network anatomy and in vivo physiology of visual cortical neurons’, *Nature*, 471(7337), pp. 177–182. Available at: https://doi.org/10.1038/nature09802.

Bogovic, J.A. *et al.* (2016) ‘Robust registration of calcium images by learned contrast synthesis’, in *2016 IEEE 13th International Symposium on Biomedical Imaging (ISBI)*. *2016 IEEE 13th International Symposium on Biomedical Imaging (ISBI 2016)*, IEEE. Available at: https://doi.org/10.1109/isbi.2016.7493463.

Boulanger-Weill, J. *et al.* (2025) ‘Correlative light and electron microscopy reveals the fine circuit structure underlying evidence accumulation in larval zebrafish’, *bioRxiv*. Available at: https://doi.org/10.1101/2025.03.14.643363.

Briggman, K.L., Helmstaedter, M. and Denk, W. (2011) ‘Wiring specificity in the direction-selectivity circuit of the retina’, *Nature*, 471(7337), pp. 183–188. Available at: https://doi.org/10.1038/nature09818.

Burgos, A. *et al.* (2018) ‘Nociceptive interneurons control modular motor pathways to promote escape behavior in’, *eLife*, 7. Available at: https://doi.org/10.7554/eLife.26016.

Bushey, D. *et al.* (2025) ‘RubyACRs enable red-shifted optogenetic inhibition in freely behaving Drosophila’. Available at: https://doi.org/10.7554/elife.108210.1.

Calderón, L.A.B., Shahidi, R. and Jékely, G. (2024) ‘Mechanism of barotaxis in marine zooplankton’. Available at: https://doi.org/10.7554/elife.94306.2.

Campbell, R.A.A. *et al.* (2013) ‘Imaging a population code for odor identity in the Drosophila mushroom body’, *The Journal of neuroscience : the official journal of the Society for Neuroscience*, 33(25), pp. 10568–10581. Available at: https://doi.org/10.1523/JNEUROSCI.0682-12.2013.

Chen, F., Tillberg, P.W. and Boyden, E.S. (2015) ‘Optical imaging. Expansion microscopy’, *Science (New York, N.Y.)*, 347(6221), pp. 543–548. Available at: https://doi.org/10.1126/science.1260088.

Chen, T.-W. *et al.* (2013) ‘Ultrasensitive fluorescent proteins for imaging neuronal activity’, *Nature*, 499(7458), pp. 295–300. Available at: https://doi.org/10.1038/nature12354.

Coates, K.E. *et al.* (2017) ‘Identified Serotonergic Modulatory Neurons Have Heterogeneous Synaptic Connectivity within the Olfactory System of’, *The Journal of neuroscience : the official journal of the Society for Neuroscience*, 37(31), pp. 7318–7331. Available at: https://doi.org/10.1523/JNEUROSCI.0192-17.2017.

Croteau-Chonka, E.C. *et al.* (2022) ‘High-throughput automated methods for classical and operant conditioning of larvae’, *eLife*, 11. Available at: https://doi.org/10.7554/eLife.70015.

Dana, H. *et al.* (2016) ‘Sensitive red protein calcium indicators for imaging neural activity’, *eLife*, 5. Available at: https://doi.org/10.7554/eLife.12727.

Dason, J.S. *et al.* (2020) ‘regulates a nociceptive-like escape behavior through a developmentally plastic sensory circuit’, *Proceedings of the National Academy of Sciences of the United States of America*, 117(38), pp. 23286–23291. Available at: https://doi.org/10.1073/pnas.1820840116.

Dorkenwald, S. *et al.* (2024) ‘Neuronal wiring diagram of an adult brain’, *Nature*, 634(8032), pp. 124–138. Available at: https://doi.org/10.1038/s41586-024-07558-y.

Dylla, K.V. *et al.* (2017) ‘Trace Conditioning in Induces Associative Plasticity in Mushroom Body Kenyon Cells and Dopaminergic Neurons’, *Frontiers in neural circuits*, 11, p. 42. Available at: https://doi.org/10.3389/fncir.2017.00042.

Eberle, A.L. *et al.* (2015) ‘High-resolution, high-throughput imaging with a multibeam scanning electron microscope’, *Journal of microscopy*, 259(2), pp. 114–120. Available at: https://doi.org/10.1111/jmi.12224.

Eichler, K. *et al.* (2017) ‘The complete connectome of a learning and memory centre in an insect brain’, *Nature*, 548(7666), pp. 175–182. Available at: https://doi.org/10.1038/nature23455.

Endo, Y. *et al.* (2025) ‘Enhanced whole-brain calcium imaging and cell identification in reveal AWC neuronal responses to 2-nonanone’, *Journal of biosciences*, 50. Available at: https://www.ncbi.nlm.nih.gov/pubmed/40619772.

Eschbach, C. *et al.* (2020) ‘Recurrent architecture for adaptive regulation of learning in the insect brain’, *Nature neuroscience*, 23(4), pp. 544–555. Available at: https://doi.org/10.1038/s41593-020-0607-9.

Eschbach, C. *et al.* (2021) ‘Circuits for integrating learned and innate valences in the insect brain’, *eLife*, 10. Available at: https://doi.org/10.7554/eLife.62567.

Eschbach, C. and Zlatic, M. (2020) ‘Useful road maps: studying Drosophila larva’s central nervous system with the help of connectomics’, *Current opinion in neurobiology*, 65, pp. 129–137. Available at: https://doi.org/10.1016/j.conb.2020.09.008.

Gallagher, B.R. and Zhao, Y. (2021) ‘Expansion microscopy: A powerful nanoscale imaging tool for neuroscientists’, *Neurobiology of disease*, 154, p. 105362. Available at: https://doi.org/10.1016/j.nbd.2021.105362.

Ganguly, I. *et al.* (2024) ‘Diversity of visual inputs to Kenyon cells of the Drosophila mushroom body’, *Nature communications*, 15(1), p. 5698. Available at: https://doi.org/10.1038/s41467-024-49616-z.

Heisenberg, M. *et al.* (1985) ‘Drosophila mushroom body mutants are deficient in olfactory learning’, *Journal of neurogenetics*, 2(1), pp. 1–30. Available at: https://doi.org/10.3109/01677068509100140.

Heisenberg, M. (2003) ‘Mushroom body memoir: from maps to models’, *Nature reviews. Neuroscience*, 4(4), pp. 266–275. Available at: https://doi.org/10.1038/nrn1074.

Hörl, D. *et al.* (2019) ‘BigStitcher: reconstructing high-resolution image datasets of cleared and expanded samples’, *Nature methods*, 16(9), pp. 870–874. Available at: https://doi.org/10.1038/s41592-019-0501-0.

Hu, C. *et al.* (2017) ‘Sensory integration and neuromodulatory feedback facilitate Drosophila mechanonociceptive behavior’, *Nature neuroscience*, 20(8), pp. 1085–1095. Available at: https://doi.org/10.1038/nn.4580.

Jenett, A. *et al.* (2012) ‘A GAL4-driver line resource for Drosophila neurobiology’, *Cell reports*, 2(4), pp. 991–1001. Available at: https://doi.org/10.1016/j.celrep.2012.09.011.

Jokura, K. *et al.* (2023) ‘Nitric oxide feedback to ciliary photoreceptor cells gates a UV avoidance circuit’. Available at: https://doi.org/10.7554/elife.91258.1.

Jovanic, T. *et al.* (2016) ‘Competitive Disinhibition Mediates Behavioral Choice and Sequences in Drosophila’, *Cell*, 167(3), pp. 858–870.e19. Available at: https://doi.org/10.1016/j.cell.2016.09.009.

Kato, S. *et al.* (2015) ‘Global brain dynamics embed the motor command sequence of Caenorhabditis elegans’, *Cell*, 163(3), pp. 656–669. Available at: https://doi.org/10.1016/j.cell.2015.09.034.

Kent, K.S., Hoskins, S.G. and Hildebrand, J.G. (1987) ‘A novel serotonin-immunoreactive neuron in the antennal lobe of the sphinx moth Manduca sexta persists throughout postembryonic life’, *Journal of neurobiology*, 18(5), pp. 451–465. Available at: https://doi.org/10.1002/neu.480180506.

Klapoetke, N.C. *et al.* (2014) ‘Independent optical excitation of distinct neural populations’, *Nature methods*, 11(3), pp. 338–346. Available at: https://doi.org/10.1038/nmeth.2836.

Kuan, A.T. *et al.* (2024) ‘Synaptic wiring motifs in posterior parietal cortex support decision-making’, *Nature*, 627(8003), pp. 367–373. Available at: https://doi.org/10.1038/s41586-024-07088-7.

Laurent, F. *et al.* (2024) ‘LarvaTagger: manual and automatic tagging of Drosophila larval behaviour’, *Bioinformatics (Oxford, England)*, 40(7). Available at: https://doi.org/10.1093/bioinformatics/btae441.

Lemon, W.C. *et al.* (2015) ‘Whole-central nervous system functional imaging in larval Drosophila’, *Nature communications*, 6, p. 7924. Available at: https://doi.org/10.1038/ncomms8924.

Li, H.-H. *et al.* (2014) ‘A GAL4 driver resource for developmental and behavioral studies on the larval CNS of Drosophila’, *Cell reports*, 8(3), pp. 897–908. Available at: https://doi.org/10.1016/j.celrep.2014.06.065.

Lillvis, J.L. *et al.* (2022) ‘Rapid reconstruction of neural circuits using tissue expansion and light sheet microscopy’, *eLife*, 11. Available at: https://doi.org/10.7554/eLife.81248.

Lin, A. *et al.* (2023) ‘Functional imaging and quantification of multineuronal olfactory

responses in', *Science advances*, 9(9), p. eade1249. Available at: https://doi.org/10.1126/sciadv.ade1249.

Marley, R. and Baines, R.A. (2011) 'Whole-cell patch recording from Drosophila larval neurons', *Cold Spring Harbor protocols*, 2011(9). Available at: https://doi.org/10.1101/pdb.prot065664.

Meissner, G.W. *et al.* (2025) 'A split-GAL4 driver line resource for Drosophila neuron types', *eLife*, 13. Available at: https://doi.org/10.7554/eLife.98405.

Nguyen, J.P. *et al.* (2016) 'Whole-brain calcium imaging with cellular resolution in freely behaving Caenorhabditis elegans', *Proceedings of the National Academy of Sciences of the United States of America*, 113(8), pp. E1074–81. Available at: https://doi.org/10.1073/pnas.1507110112.

Ohyama, T. *et al.* (2015) 'A multilevel multimodal circuit enhances action selection in Drosophila', *Nature*, 520(7549), pp. 633–639. Available at: https://doi.org/10.1038/nature14297.

Phelps, J.S. *et al.* (2021) 'Reconstruction of motor control circuits in adult Drosophila using automated transmission electron microscopy', *Cell*, 184(3), pp. 759–774.e18. Available at: https://doi.org/10.1016/j.cell.2020.12.013.

Polizos, N.T. *et al.* (2024) 'Drosophila larvae form appetitive and aversive associative memory in response to thermal conditioning', *PloS one*, 19(9), p. e0303955. Available at: https://doi.org/10.1371/journal.pone.0303955.

Randi, F. *et al.* (2023) 'Neural signal propagation atlas of Caenorhabditis elegans', *Nature*, 623(7986), pp. 406–414. Available at: https://doi.org/10.1038/s41586-023-06683-4.

Ryan, K., Lu, Z. and Meinertzhagen, I.A. (2016) 'The CNS connectome of a tadpole larva of Ciona intestinalis (L.) highlights sidedness in the brain of a chordate sibling', *eLife*, 5. Available at: https://doi.org/10.7554/eLife.16962.

Saalfeld, S. *et al.* (2009) 'CATMAID: collaborative annotation toolkit for massive amounts of image data', *Bioinformatics* , 25(15), pp. 1984–1986. Available at: https://doi.org/10.1093/bioinformatics/btp266.

Scheffer, L.K. *et al.* (2020) 'A connectome and analysis of the adult Drosophila central brain', *eLife*, 9. Available at: https://doi.org/10.7554/eLife.57443.

Schmidt, U. *et al.* (2018) 'Cell detection with star-convex polygons', in *Medical Image Computing and Computer Assisted Intervention – MICCAI 2018*. Cham: Springer International Publishing (Lecture notes in computer science), pp. 265–273. Available at: https://doi.org/10.1007/978-3-030-00934-2_30.

Schrödel, T. *et al.* (2013) 'Brain-wide 3D imaging of neuronal activity in Caenorhabditis elegans with sculpted light', *Nature methods*, 10(10), pp. 1013–1020. Available at: https://doi.org/10.1038/nmeth.2637.

Seligman, A.M., Wasserkrug, H.L. and Hanker, J.S. (1966) 'A new staining method (OTO) for enhancing contrast of lipid--containing membranes and droplets in osmium tetroxide--fixed tissue with osmiophilic thiocarbohydrazide(TCH)', *The Journal of cell biology*, 30(2), pp. 424–432. Available at: https://doi.org/10.1083/jcb.30.2.424.

Spindler, S.R. and Hartenstein, V. (2010) 'The Drosophila neural lineages: a model system

to study brain development and circuitry', *Development genes and evolution*, 220(1-2), pp. 1–10. Available at: https://doi.org/10.1007/s00427-010-0323-7.

Svara, F. *et al.* (2022) 'Automated synapse-level reconstruction of neural circuits in the larval zebrafish brain', *Nature methods*, 19(11), pp. 1357–1366. Available at: https://doi.org/10.1038/s41592-022-01621-0.

Takagi, S. *et al.* (2017) 'Divergent Connectivity of Homologous Command-like Neurons Mediates Segment-Specific Touch Responses in Drosophila', *Neuron*, 96(6), pp. 1373–1387.e6. Available at: https://doi.org/10.1016/j.neuron.2017.10.030.

Takemura, S.-Y. *et al.* (2023) 'A connectome of the male*Drosophila*ventral nerve cord', *bioRxiv*. Available at: https://doi.org/10.1101/2023.06.05.543757.

Thum, A.S. and Gerber, B. (2019) 'Connectomics and function of a memory network: the mushroom body of larval Drosophila', *Current opinion in neurobiology*, 54, pp. 146–154. Available at: https://doi.org/10.1016/j.conb.2018.10.007.

Tomer, R. *et al.* (2012) 'Quantitative high-speed imaging of entire developing embryos with simultaneous multiview light-sheet microscopy', *Nature methods*, 9(7), pp. 755–763. Available at: https://doi.org/10.1038/nmeth.2062.

Toyoshima, Y. *et al.* (2020) 'Neuron ID dataset facilitates neuronal annotation for whole-brain activity imaging of C. elegans', *BMC biology*, 18(1), p. 30. Available at: https://doi.org/10.1186/s12915-020-0745-2.

Tracey, W.D., Jr *et al.* (2003) 'painless, a Drosophila gene essential for nociception', *Cell*, 113(2), pp. 261–273. Available at: https://doi.org/10.1016/s0092-8674(03)00272-1.

Verasztó, C. *et al.* (2017) 'Ciliomotor circuitry underlying whole-body coordination of ciliary activity in the Platynereis larva', *eLife*, 6. Available at: https://doi.org/10.7554/eLife.26000.

Verasztó, C. *et al.* (2020) 'Whole-animal connectome and cell-type complement of the three-segmented Platynereis dumerilii larva', *bioRxiv* [Preprint]. Available at: https://www.biorxiv.org/content/10.1101/2020.08.21.260984v1.abstract.

Vogelstein, J.T. *et al.* (2014) 'Discovery of brainwide neural-behavioral maps via multiscale unsupervised structure learning', *Science (New York, N.Y.)*, 344(6182), pp. 386–392. Available at: https://doi.org/10.1126/science.1250298.

Walton, J. (1979) 'Lead asparate, an en bloc contrast stain particularly useful for ultrastructural enzymology', *The journal of histochemistry and cytochemistry: official journal of the Histochemistry Society*, 27(10), pp. 1337–1342. Available at: https://doi.org/10.1177/27.10.512319.

van der Walt, S. *et al.* (2014) 'scikit-image: image processing in Python', *PeerJ*, 2, p. e453. Available at: https://doi.org/10.7717/peerj.453.

White, J.G. *et al.* (1986) 'The structure of the nervous system of the nematode Caenorhabditis elegans', *Philosophical transactions of the Royal Society of London. Series B, Biological sciences*, 314(1165), pp. 1–340. Available at: https://doi.org/10.1098/rstb.1986.0056.

Winding, M. *et al.* (2023) 'The connectome of an insect brain', *Science (New York, N.Y.)*, 379(6636), p. eadd9330. Available at: https://doi.org/10.1126/science.add9330.

Witvliet, D. *et al.* (2021) 'Connectomes across development reveal principles of brain

maturation', *Nature*, 596(7871), pp. 257–261. Available at: https://doi.org/10.1038/s41586-021-03778-8.

Xu, C.S. *et al.* (2017) 'Enhanced FIB-SEM systems for large-volume 3D imaging', *eLife*, 6. Available at: https://doi.org/10.7554/eLife.25916.

Yemini, E. *et al.* (2021) 'NeuroPAL: A Multicolor Atlas for Whole-Brain Neuronal Identification in C. elegans', *Cell*, 184(1), pp. 272–288.e11. Available at: https://doi.org/10.1016/j.cell.2020.12.012.

Zhang, Y. *et al.* (2023) 'Fast and sensitive GCaMP calcium indicators for imaging neural populations', *Nature*, 615(7954), pp. 884–891. Available at: https://doi.org/10.1038/s41586-023-05828-9.

Zheng, Z. *et al.* (2018) 'A Complete Electron Microscopy Volume of the Brain of Adult Drosophila melanogaster', *Cell*, 174(3), pp. 730–743.e22. Available at: https://doi.org/10.1016/j.cell.2018.06.019.

Author contributions:

NR: Conceptualisation, Formal analysis, Investigation, Methodology, Validation, Project administration, Visualization, Writing – original draft, Writing – review and editing, Funding acquisition.
CW: Methodology
MSC: Data curation. Software.
KW: Validation. Methodology. Investigation.
SP: Resources
CSX: Resources
AC: Data curation.
HH: Conceptualisation. Funding acquisition. Resources.
AC: Data curation. Funding acquisition.
PJK: Conceptualisation, Software, Project administration, Data curation. Resources, Funding acquisition.
MZ: Conceptualisation. Project administration, Resources, Writing – original draft, Writing – review and editing, Supervision, Funding acquisition.

Declaration of Interest

The authors declare no competing interests.

Tables

Table 1: Cell lineages that are 2-5 hops downstream of Basins and whether they were identified in the LSM whole-brain imaging dataset.

Cell lineage	No. of hops	Identified in functional imaging
BLD2-4 L	2	yes
BLAv1/2 p L	2	yes
BLVa3/4 a L	2	yes
BLVp2 L	2	yes
CP1 v L	2	yes
CP2/3 v L	2	yes
DPLp1/2 L	2	yes
DPMm2 L	2	yes
DPMpl3 L	2	yes
BLAv1/2 a L	2	yes
BLAvm p L	2	no
BLD5/6 L	2	no
BLP3/4 b L	2	no
BLVp1 L	2	no
DPMl1 L	2	no
BLAv1/2 a L	3	yes
BLAv1/2 l L	3	yes
BLAv1/2 p L	3	yes
BLD2-4 L	3	yes
BLP1/2 a L	3	yes
BLVa3/4 a L	3	yes
BLVa3/4 t L	3	yes
BLVp1 L	3	yes
BLVp2 L	3	yes
CM1/3 L	3	yes
CM4 L	3	yes
CP1 v L	3	yes
CP2/3 d L	3	yes
CP2/3 v L	3	yes
DALv2/3 L	3	yes
DPLal1-3 L	3	yes
DPLl1-3 a L	3	yes
DPMm2 L	3	yes
DPMpl3 L	3	yes
BAla1/2 L	3	no
BAla3/4 L	3	no
BAmd1 L	3	no
BAmd2 L	3	no
BAmv1/2 L	3	no
BLAd1-4 L	3	no
BLAl L	3	no
BLAvm a L	3	no
BLAvm p L	3	no
BLD5/6 L	3	no
BLP3/4 b L	3	no

BLVa1/2 a L	3	no
CP1 d L	3	no
CP4 L	3	no
DALcl1/2 v L	3	no
DALcm1/2 m L	3	no
DALd L	3	no
DALl1 L	3	no
DALv1 L	3	no
DALv2/3 acc lat L	3	no
DALv2/3 acc med L	3	no
DALv2/3 acc ven L	3	no
DALv2/3 acc ven lat L	3	no
DPLam L	3	no
DPLc4 L	3	no
DPLc5 a L	3	no
DPLd L	3	no
DPMl1 L	3	no
DPMl2 L	3	no
DPMl3/4 p L	3	no
DPMm1 L	3	no
DPMpl1/2 L	3	no
BAlc L	4	yes
BAlp1-3 L	4	yes
BLAv1/2 a L	4	yes
BLAv1/2 l L	4	yes
BLAv1/2 p R	4	yes
BLD2-4 L	4	yes
BLP1/2 a L	4	yes
BLP1/2 b L	4	yes
BLVa3/4 a L	4	yes
BLVa3/4 b L	4	yes
BLVa3/4 t L	4	yes
BLVp1 L	4	yes
BLVp2 L	4	yes
CM1/3 L	4	yes
CM4 L	4	yes
CP1 v L	4	yes
CP2/3 d L	4	yes
CP2/3 v L	4	yes
DALv2/3 L	4	yes
DPLal1-3 L	4	yes
DPLl1-3 a L	4	yes
DPLp1/2 L	4	yes
DPMm2 L	4	yes
DPMpl3 L	4	yes
BAla1/2 L	4	no

BAla3/4 L	4	no
BAmd1 L	4	no
BAmd2 L	4	no
BAmv1/2 L	4	no
BLAd1-4 L	4	no
BLAI L	4	no
BLAv1/2 v L	4	no
BLAvm a L	4	no
BLAvm c L	4	no
BLAvm p L	4	no
BLD1 L	4	no
BLP3/4 a L	4	no
BLP3/4 b L	4	no
BLVa1/2 a L	4	no
BLVa1/2 b L	4	no
CP1 d L	4	no
CP4 L	4	no
DALcl1/2 d L	4	no
DALcl1/2 v L	4	no
DALcm1/2 m L	4	no
DALcm1/2 v L	4	no
DALd L	4	no
DALI1 L	4	no
DALv1 L	4	no
DALv2/3 acc lat L	4	no
DALv2/3 acc med L	4	no
DALv2/3 acc ven L	4	no
DALv2/3 acc ven lat L	4	no
DAMd1 L	4	no
DAMd2/3 L	4	no
DAMv1/2 L	4	no
DILP L	4	no
DPLam L	4	no
DPLc1 L	4	no
DPLc3 L	4	no
DPLc4 L	4	no
DPLc5 a L	4	no
DPLc5 p L	4	no
DPLd L	4	no
DPLI1-3 i L	4	no
DPLI1-3 L	4	no
DPLm1 L	4	no
DPLm2 L	4	no
DPMI1 L	4	no
DPMI2 L	4	no
DPMI3/4 p L	4	no

DPMm1 L	4	no
DPMpl1/2 L	4	no
DPMpm1 L	4	no
DPMpm2 L	4	no
BAlc L	5	yes
BAlp1-3 L	5	yes
BAmas1/2 L	5	yes
BLAv1/2 a L	5	yes
BLAv1/2 l R	5	yes
BLAv1/2 p L	5	yes
BLD2-4 L	5	yes
BLP1/2 a L	5	yes
BLP1/2 b L	5	yes
BLVa3/4 a L	5	yes
BLVa3/4 b L	5	yes
BLVa3/4 t L	5	yes
BLVp1 L	5	yes
BLVp2 L	5	yes
CM1/3 L	5	yes
CM4 L	5	yes
CP1 v L	5	yes
CP2/3 d L	5	yes
CP2/3 v L	5	yes
DALv2/3 L	5	yes
DPLal1-3 L	5	yes
DPLl1-3 a L	5	yes
DPLp1/2 L	5	yes
DPMm2 L	5	yes
DPMpl3 L	5	yes
KeC L	5	yes
BAla1/2 L	5	no
BAla3/4 L	5	no
BAlp4 L	5	no
BAlv L	5	no
BAmd1 L	5	no
BAmd2 L	5	no
BAmv1/2 L	5	no
BAmv3 L	5	no
BLAd1-4 L	5	no
BLAl L	5	no
BLAvm a L	5	no
BLAvm c L	5	no
BLD1 R	5	no
BLP3/4 a L	5	no
BLP3/4 b L	5	no
BLVa1/2 a L	5	no

BLVa1/2 b L	5	no
CP1 d L	5	no
DALcl1/2 v L	5	no
DALcm1/2 v L	5	no
DALd L	5	no
DALl1 L	5	no
DALv1 L	5	no
DALv2/3 acc ven L	5	no
DAMd1 L	5	no
DAMv1/2 L	5	no
DILP L	5	no
DPLam L	5	no
DPLc1 L	5	no
DPLc4 L	5	no
DPLc5 p L	5	no
DPLd L	5	no
DPLl1-3 i L	5	no
DPLm1 L	5	no
DPLm2 L	5	no
DPMl1 L	5	no
DPMl1 R	5	no
DPMl2 L	5	no
DPMl3/4 a L	5	no
DPMl3/4 p L	5	no
DPMm1 L	5	no
DPMpl1/2 L	5	no
DPMpm1 L	5	no
DPMpm2 L	5	no

Table 2: Identified brain neurons with their corresponding cell lineage, cell type, sensory modality, hub-neuron identity, and synaptic connectivity (synaptic threshold: 0.01; *synaptic threshold: ≥3 synapses). Candidate neurons, which could not be uniquely identified, are listed individually. Hub neurons are defined as having ≥20 in- or out-degree (Winding *et al.*, 2023).

skid	Publication name	Cell lineage	Cell type	Sensory modality	Synaptic connectivity downstream Basin	hub neuron
3044500	DNsez-1_stop	DPMm2	DN-SEZ	3rd order: noci, mechano	3-hop	yes
9234420	DNsez-3	BLAv1/2	DN-SEZ	3rd order: noci, mechano	3-hop	yes
17728922	DNsez-3	BLAv1/2	DN-SEZ	3rd order: noci, mechano	3-hop	yes
8723983	DNvnc-13	CM1/3	DN-VNC	4th order: gustatory, olfactory	5-hop	no
17075832	DNvnc-14	BAlp 1-3	DN-VNC	3rd order: gustatory	4-hop	no
7439913	DNvnc-15	BAlp 1-3	DN-VNC	3rd order: gustatory	4-hop	no
10915553	DNvnc-16	CM4	DN-VNC	3rd order: noci	3-hop	no
10609443	DNvnc-17	CM4	DN-VNC	3rd order: noci, mechano	3-hop	no
17732270	DNvnc-18	CM4	DN-VNC	3rd order: mechano	4-hop	no
7227010	DNvnc-19	CM4	DN-VNC	3rd order: noci	3-hop	no
10945795	DNvnc-20	BLVp2	DN-VNC	3rd order: noci, mechano	3-hop	no
15588711	DNvnc-20	BLVp2	DN-VNC	3rd order: noci, mechano	3-hop	no
na	Kenyon cells	KC	KC	na	5-hop*	no
na	Kenyon cells	KC	KC	na	5-hop*	no
na	Kenyon cells	KC	KC	na	5-hop*	no
na	Kenyon cells	KC	KC	na	5-hop*	no
na	Kenyon cells	KC	KC	na	5-hop*	no
5118060	LHN-32	BLAv1/2	LHNs	2nd mechano, 3rd olfactory	4-hop	yes
7910624	MBON-q1	BLAv1/2	MBON	3rd order: mechano, respiratory	5-hop	no
17728723	Lasso-top 1	BAlp 1-3	na	3rd order: gustatory	7-hop	no
17728730	Lasso-top 2	BAlp 1-3	na	3rd order: gustatory	5-hop	no
8809171	Lasso-top 3	BAlp 1-3	na	4th order: noci, gustatory, olfactory, thermio-warm	5-hop	no
14270761	Tel-like 1	BLVp1	na	3rd order: noci	3-hop	no
5744502	Noose 1	BLVp2	na	3rd order: mechano	4-hop	no
6541149	somPN 6	BLAv1/2	PN-somato	2nd order: noci	2-hop	no
6623089	pre-DNvnc-18	BLAv1/2	pre-DN-VNC	2nd order: noci	3-hop	no
16931001	pre-DNvnc-19	BLAv1/2	pre-DN-VNC	3rd order: noci, mechano	3-hop	no
11291653	somPN 7	BLAv1/2	PN-somato	2nd order: noci	4-hop	no
11263687	somPN 8	BLAv1/2	PN-somato	2nd order: noci	2-hop	yes
20730780	somPN 9	BLAv1/2	PN-somato	2nd order: noci	2-hop	no

Table 3: Skeleton IDs (Skids) and names of previously published neurons.

Left skid	Right skid	Neuron name
1678567	6153877	DNvnc-21
10728328	18464581	DNvnc-22
17165755	13727202	DNvnc-23
16851496	16339338	DNvnc-24
5763407	10945111	DNvnc-25
15365184	5512988	DNvnc-26
13749806	14034206	DNvnc-27
8834812	18970354	A02
7766185	7934152	SeIN134
1767828	4139768	A12m
4081479	5336476	A19c
4740178	4833168	A05q
21250110	9640873	A10j
4680995	17806341	LHN-4
14319185	8565131	CN-57
16486385	11178891	CN-46
10540188	8932110	Cheech
12498338	3913629	CN-50
12476851	16070049	CN-1
17434825	16485079	CN-47
3044500	6317793	DNsez-1_stop
17728922	9234420	DNsez-3
8723983	16115255	DNvnc-13
17075832	14039007	DNvnc-14
7439913	15934458	DNvnc-15
10915553	11905911	DNvnc-16
10609443	6114695	DNvnc-17
17732270	6125806	DNvnc-18
7227010	16115575	DNvnc-19
15588711	10945795	DNvnc-20
5118060	15605987	LHN-32
7910624	7897469	MBON-q1
17728723	13084891	Lasso-top 1
17728730	17629213	Lasso-top 2
8809171	18187865	Lasso-top 3
14270761	9103710	Tel-like 1
5744502	1805406	Noose 1
6541149	10079731	somPN 6
6623089	17897230	pre-DNvnc-18
16931001	8709865	pre-DNvnc-19
11291653	8412625	somPN 7
11263687	6692908	somPN 8
20730780	9202326	somPN 9
4966994	16578252	pre-DNvnc-20
13849557	6143930	CSD

Table 4: Identified neurons per lineage pair.

Lineage	No. of Neurons (Sample Brain)	No. of Neurons (Reference Brain)	%
BLP1/2	4	102	3.9
BLVa3/4	9	99	9.1
BLAv1/2	30	111	27.0
CM1/3	1	95	1.1
CM4	4	184	2.2
CP1 v	1	62	1.6
CP2/3v	1	80	1.3
DALv 2/3	1	42	2.4
DPLal 1-3	2	82	2.4
DPLl 1-3a	1	24	4.2
DPLp 1/2	4	26	15.4
DPMm2	2	46	4.3
CP2/3 d	1	48	2.1
DPMpl3	1	30	3.3
KC	5	223	2.2
BLVp1, BLVp2	12	62	19.4
Balc	1	86	1.2
BLD2-4	17	72	23.6
BAlp1-3	3	68	4.4
BAmas1/2	1	98	1.0
Sum	101	1640	
Mean	5.05	82	6.6
Median	2	76	2.9

Table 5: Number of neurons 2-hop downstream of basins per lineage pair.

Lineage	No. of Neurons	2-hop downstream of basins	%
BLAv1/2	111	29	26.1
BLVa3/4	99	20	20.2
BLVp1, BLVp2	62	14	22.6
BLD2-4	72	8	11.1
BLP1/2	102	6	5.9
CM1/3	95	2	2.1
CM4	184	3	1.6
CP1 v	62	10	16.1
CP2/3v	80	4	5.0
DALv 2/3	42	0	0.0
DPLal 1-3	82	13	15.9
DPLl 1-3a	24	0	0.0
DPLp 1/2	26	3	11.5
DPMm2	46	4	8.7
CP2/3d	48	0	0.0
DPMpl3	30	3	10.0
KC	223	0	0.0
Balc	86	1	1.2
BAlp1-3	68	0	0.0
BAmas1/2	98	3	3.1